

Progressive-Resolution Policy Distillation: Leveraging Coarse-Resolution Simulation for Time-Efficient Fine-Resolution Policy Learning

Yuki Kadokawa¹, Hirotaka Tahara^{1,2}, Takamitsu Matsubara¹

Abstract—In earthwork and construction, excavators often encounter large rocks mixed with various soil conditions, requiring skilled operators. This paper presents a framework for achieving autonomous excavation using reinforcement learning (RL) through a rock excavation simulator. In the simulation, resolution can be defined by the particle size/number in the whole soil space. Fine-resolution simulations closely mimic real-world behavior but demand significant calculation time and challenging sample collection, while coarse-resolution simulations enable faster sample collection but deviate from real-world behavior. To combine the advantages of both resolutions, we explore using policies developed in coarse-resolution simulations for pre-training in fine-resolution simulations. To this end, we propose a novel policy learning framework called Progressive-Resolution Policy Distillation (PRPD), which progressively transfers policies through some middle-resolution simulations with conservative policy transfer to avoid domain gaps that could lead to policy transfer failure. Validation in a rock excavation simulator and nine real-world rock environments demonstrated that PRPD reduced sampling time to less than 1/7 while maintaining task success rates comparable to those achieved through policy learning in a fine-resolution simulation.

I. INTRODUCTION

Autonomous excavation has been studied to meet the rising demand for earthwork and construction [1]. In excavation, especially in mountainous areas, quarry sites, and construction sites, large rocks are often mixed with sand, gravel, and pebbles in the soil [2]. Operating excavators must have advanced operational expertise to find, collect, and transport these rocks [3]. For rock excavation, excavators must efficiently lift and move rocks using a bucket. This involves non-grasping bucket motion while considering forces from rock-soil-bucket interactions, a task only skilled operators can perform [4]. Due to the varied shapes and sizes of rocks, automating rock excavation with simple autonomous control policies is challenging [5].

Reinforcement learning (RL) is potentially useful to learn optimal actions from diverse state-action transitions caused by various rocks [6]. RL learns control policies from interaction samples between a robot and the environment. Thus, simulators are commonly used since real-world sampling requires significant manual efforts to set up various types of soil and objects [7]. In previous simulation work, computational mechanics and particle methods have been used. Computational mechanics, which discretize terrain into elements, are suitable for simple terrains but struggle with

This work was supported by JST Moonshot Research and Development, Grant Number JPMJMS2032. ¹ Nara Institute of Science and Technology, Nara 630-0192, Japan. ² Kobe City College of Technology, Hyogo 651-2194, Japan. kadokawa.yuki@naist.ac.jp, h-tahara@kobe-kosen.ac.jp, takam-m@is.naist.jp

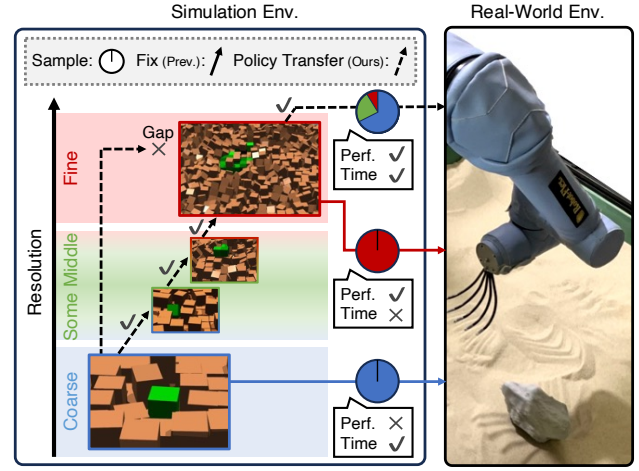


Fig. 1: Overview of proposed framework: Fine-resolution simulations yield high policy performance but require long learning times, while coarse-resolution simulations allow for quick learning but perform poorly in sim-to-real transfer. Our framework starts with coarse-resolution simulations for quick learning and progressively transfers policies to fine-resolution simulations. Progressive resolution shift with conservative policy transfer is applied to avoid large domain gaps that could lead to policy transfer failure. This approach balances learning time with real-world performance.

complex terrains involving rocks or nonlinear phenomena [7]. Conversely, particle methods model materials as individual particles and simulate their interactions, effectively reproducing complex phenomena like friction, collisions, and soil deformation [8]. This makes particle methods suitable for simulating complex terrains that include rocks.

While particle-based simulations can be accurate and realistic, they face challenges in calculation time for our RL application, particularly as *spatial resolution* improves. This resolution can be defined by the particle size/number in the whole soil space, with smaller particle sizes (more amounts of particles) allowing for a more detailed particle representation of the soil space and obtaining a finer resolution. Fine resolution leads to complex particle interactions, making it impractical to collect the vast samples needed for RL in a reasonable calculation time [9]. Ideally, the resolution should be coarsened until the simulator is sufficiently fast; however, simulation deviates from real-world behavior, utilizing the learned policies ineffective in real-world environments.

As shown in Fig. 1, we explore using policies developed in coarse-resolution simulations for pre-training in fine-resolution simulations, even though these policies cannot work in real-world settings. This approach potentially reduces sampling time compared to using only fine-resolution simulations since coarse-resolution simulations can be calculated in a shorter time. However, behaviors in different

resolution simulations typically deviate due to domain gaps, making it challenging to utilize coarse-resolution simulations for pre-training. Therefore, by transferring policies progressively through some middle resolutions and by transferring policies gradually while checking the stability of the policy updates instead of transferring policies all at once, we could effectively transition these policies to simulations that closely resemble real-world settings.

We propose a novel policy learning framework called Progressive-Resolution Policy Distillation (PRPD) for achieving time-efficient policy learning of fine-resolution simulations by utilizing coarse-resolution simulations effectively. PRPD progressively improves simulation resolution while learning and transferring policies at each stage. PRPD uses a conservative policy transfer scheme to regularize policies, stabilizing policy transfer across different resolution simulations having different behaviors. We demonstrated the effectiveness of PRPD by constructing a variable-resolution rock excavation simulator. PRPD reduced sampling time to less than 1/7 while maintaining task success rates comparable to policy learning in a fine-resolution simulation. Furthermore, in evaluations of the learned policies within a real-world environment containing nine types of rocks, PRPD achieved rock excavation in approximately 90 % of scenarios. As an impact of this study, achieving realistic simulations of complex environments, such as excavation tasks, remains challenging. While advances in computational resources and simulation technologies may alleviate simulation time issues, simulating real-world environments accurately remains prohibitively costly and will still face resource limits. This study offers insights into addressing these challenges by improving policy-learning efficiency.

II. RELATED WORKS

A. Learning Excavation Policy

This section describes several methods for acquiring control policies for robotic excavations with soil and rocks. Previous works have proposed the following three approaches.

Learning in Real-world: Learning rock-excavation tasks in real-world environments requires extensive sampling time. These works have modeled soil and rock behavior from limited samples to learn control policies [5]. However, accurately modeling rock behavior requires interaction samples for various rock shapes. The vast number of combinations makes it difficult to apply this method to multiple shapes due to sampling costs, so previous research has only obtained policies for a single rock shape.

Learning in Simulation by Computational Mechanics: These works simulate soil behavior in response to bucket movements using computational mechanics and collect learning samples from model interactions [7]. The finite element method divides soil into small elements and solves for displacement, stress, and strain. Deformation analysis uses soil mechanics equations to analyze deformation and failure. These works are suitable for simulating simple terrain because they numerically discretize and simulate terrain, but

they have difficulty accurately reproducing complex terrain involving rocks and nonlinear phenomena.

Learning in Simulation by Particle Method: These works adopt the particle method that models materials as individual particles and directly simulates the interactions between them [10]. This enables detailed simulation of rock and soil behavior, and approximates complex physical phenomena such as inter-particle friction, collision, and soil deformation separately. However, calculating interactions between multiple particles is time-consuming, making it difficult to collect many learning samples.

We aim to establish learning policies applicable to various rock shapes by utilizing a particle-based simulator capable of achieving this aim. To address the sampling time challenge, we propose a novel policy learning framework that enables the short-time learning sample collection from various rock shapes, thereby achieving multiple-shape rock excavation.

B. Excavation Simulator by Particle Method

Excavation simulators with a large number of particle interactions require extensive calculation time [10]. The following paragraphs describe previous works that employed three approaches to accelerate calculations and comparisons with our developed simulator.

Static Adjustment of Resolution: To reduce the calculation time for particle interactions, which make up the majority of simulation calculations, efforts have focused on generating environments limited to specific work areas and approximating many soil particles with fewer macro particles [11]. These strategies have decreased the necessary memory resources and sampling time. However, there are limits to how much the resolution can be reduced without diverging from real-world behavior.

Dynamic Adjustment of Resolution: Some works accelerate simulations by dynamically changing the resolution [8]. They dynamically estimate the work area, splitting particles in fine-resolution regions and merging particles in coarse-resolution areas, thereby reducing calculation time. While this approach achieves acceleration, focusing fine resolution only in the work area still requires significant resources and calculation time.

Parallel Calculation of Particles: Recently, frameworks like Isaac Gym and Isaac Sim have been developed to rapidly simulate robot environments using GPUs, significantly accelerating sampling time [11]. In excavation environments, these achieve faster calculations by parallelizing the calculation of multiple particle interactions. However, generating a vast number of particles within the simulation requires substantial GPU memory, making it difficult to create parallel environments that can further reduce sampling time [12].

Our Developed Simulator: The simulator developed in this paper incorporates equivalents of the three acceleration techniques of the previous works: (1) approximating soil with micro particles, (2) generating only the work area for fine-resolution simulation, and (3) using Isaac Gym for GPU acceleration. The details of our simulator are described in Sec. V-D.

Despite these advancements in simulation acceleration, they remain insufficient for the vast sample collection required in RL [8]. The goal of this paper is not to develop realistic simulations but to learn policies of realistic simulations. To shorten sampling time, we use both fine-resolution simulations that take longer to calculate and extremely coarse-resolution simulations that require less calculation time.

C. Sample Efficient Reinforcement Learning Methods

Several methods improve sample efficiency in RL. Model-based RL uses a learned model of the environment's dynamics [13]. Auxiliary tasks and autoencoders extract features from observations [13, 14]. Data augmentation enhances information content by transforming observation samples [15]. Ensemble learning improves robustness and adaptability with multiple models [14]. Imitation learning trains policies from demonstrations, and reward function learning from small demonstration sets reduces human effort [9]. Off-policy RL such as soft actor-critic (SAC) efficiently explores and learns by reusing past interaction data [16].

Various methods have improved RL's "sample efficiency" by extracting more information from each sample or increasing update times to maximize sample utilization. However, these approaches often come with computational overhead, such as increased calculation time and resource demands by adding learning components, which can compromise "time efficiency," the overall training time for policy learning.

Our approach can be interpreted as a type of curriculum reinforcement learning (CRL) since it also involves gradually changing the tasks from simple to complex [17]. In detail, CRL gradually increases task difficulty, reducing the sample requirements compared to learning solely on complex tasks. However, to the best of our knowledge, our approach is the first to treat differences in the spatial resolution of complex simulations as distinct tasks.

III. PRELIMINARIES

A. Reinforcement Learning

Reinforcement Learning (RL) is formulated as a Markov Decision Process (MDP) \mathcal{M} . MDP is defined by the state space \mathcal{S} , action space \mathcal{A} , state transition probability $P(s'|s, a)$, and reward function $R(s, a)$, represented as $\mathcal{M} = (\mathcal{S}, \mathcal{A}, P, R)$. The agent selects an action $a \in \mathcal{A}$ in the current state $s \in \mathcal{S}$ and, as a result, observes the next state $s' \in \mathcal{S}$ and reward $r \in \mathbb{R}$. The goal in an MDP is to find a policy $\pi(a|s)$ that maximizes the expected cumulative reward $J(\pi)$, given by $J(\pi) = \mathbb{E}_\pi [\sum_{t=0}^{\infty} \gamma^t r_t]$, $\gamma \in [0, 1]$ is the discount factor.

To maximize the expected cumulative reward $J(\pi)$, policy gradient methods can be used, where the objective function is defined as $J(\pi) = \mathbb{E}_\pi [\sum_{t=0}^{\infty} A(s_t, a_t)]$, where $A(s, a) = Q(s, a) - V(s)$ is the advantage function. The action value function $Q(s, a) = \mathbb{E}_\pi [\sum_{t=0}^{\infty} \gamma^t r_t | s_0 = s, a_0 = a]$ represents the expected cumulative reward when action a is taken in state s . The state value function $V(s) = \mathbb{E}_\pi [\sum_{t=0}^{\infty} \gamma^t r_t | s_0 = s]$ represents the expected cumulative reward starting from state s and following policy $\pi(s, a)$. These functions are typically approximated using function

approximators, specifically neural networks, which parameterize the policy as $\pi(s, a; \theta)$, the state value function as $V(s; \phi)$, and the action value function as $Q(s, a; \psi)$, where θ , ϕ , and ψ represent their respective parameters.

Typically, RL methods learn an optimal policy by iteratively conducting the following two steps: (1) collecting samples (s, a, r, s') with the policy π into a rollout buffer \mathcal{D}_i , and (2) updating the policy using these samples. This iteration number is denoted as i , and the parameter update number is denoted as k .

B. Conservative Policy Update in Reinforcement Learning

In RL, there are various errors such as function approximation errors and observation noise, and attempts have been made to learn policies that are robust to these errors. Conservative Policy Iteration (CPI) is one example, which is designed to achieve more stable policy updates by relaxing the policy updates scheme [18].

In CPI, the policy update is modified to make it more conservative by introducing a mixing coefficient α . The new policy π_{k+1} is a mixture of the current policy π_k and the greedy policy $\mathcal{G}(Q_k)(s) = \arg \max_a Q_k(s, a)$:

$$\pi_{k+1}(s, a) \leftarrow (1 - \alpha_{k+1})\pi_k(s, a) + \alpha_{k+1}\mathcal{G}(Q_k)(s), \quad (1)$$

where $0 \leq \alpha_{k+1} \leq 1$. This approach stabilizes policy learning by mitigating abrupt policy changes.

CPI comes with strong theoretical guarantees that ensure the policy value improves monotonically under certain conditions; if the function approximation error is bounded and the mixing coefficient α_k is chosen appropriately, the expected value of the policy is guaranteed to improve. Specifically, the mixing rate can be selected as:

$$\alpha_{k+1} = \frac{(1 - \gamma)}{4R} \sum_{s \in \mathcal{S}} d_\mu^{\pi_{k-1}}(s) \sum_{a \in \mathcal{A}} \pi_k(a|s) A_k(s, a), \quad (2)$$

where $d_\mu^{\pi_{k-1}}(s)$ is the discounted state visitation distribution under policy π_{k-1} starting from initial state distribution μ , R is the maximum reward [18].

IV. PROGRESSIVE-RESOLUTION POLICY DISTILLATION

We propose a novel policy learning framework called Progressive-Resolution Policy Distillation (PRPD) to achieve time-efficient policy learning of fine-resolution simulations by utilizing coarse-resolution simulations effectively. An overview of the proposed PRPD framework is shown in Fig. 1. PRPD progressively improves simulation resolution and transfers policies at each stage. By transferring policies progressively through some middle resolutions and by transferring policies gradually while checking the stability of the policy updates instead of transferring policies all at once, we effectively transition these policies to simulations that closely resemble real-world settings. PRPD incorporates iterations of the following two steps: 1) Resolution Scheduling and 2) Policy Learning.

Simulator Assumption: To enable policy transfer, our framework follows some simulator assumptions. We assume that resolution-affected elements do not impact observations

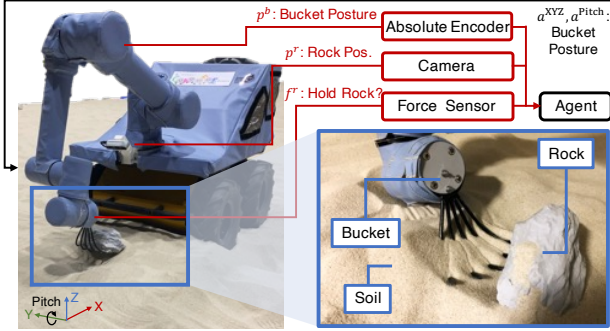


Fig. 2: Our experimental rock excavation setup: The excavator operates a bucket attached to its arm to remove rocks from the soil. Inputs to the control policy include the bucket's posture p^b (position and rotation) from the excavator's absolute encoder, rock coordinates p^r estimated by the camera, and the presence of rocks in the bucket f^r estimated by the force sensor. The output of the control policy is the position a^{XYZ} and rotation of the bucket a^{Pitch} . The fork-shaped bucket is designed to imitate the features of skeleton buckets.

or actions. The policies' objectives remain the same, with only the resolution differing, so the reward function is kept identical. This framework supports policy learning in high-resolution simulations, assuming that behavior is less accurate at coarser resolutions and becomes finer as resolution improves.

RL Scheme Assumption: PRPD assumes an actor-critic structure for the RL scheme, it requires policy π and value function Q for estimating α . Applicable learning methods include the latest DRLs such as PPO [19] and SAC [16].

A. Resolution Scheduling

1) Execution Flow: The simulation resolution $\Delta \in \mathbb{R}$ is scheduled based on the progress of policy learning by the resolution scheduler. Specifically, the resolution remains constant until the policy achieves the task, at which point it is progressively improved by Δ_R . The success rate is evaluated across all results of each iteration, with the success defined by meeting the threshold τ . The simulation generator then creates the simulator $\mathcal{M}^{(n)}$ according to the scheduled resolution Δ .

2) Scheduling Setups: PRPD creates a simulation environment represented as MDPs $\mathcal{M}^{(1)}, \mathcal{M}^{(2)}, \dots, \mathcal{M}^{(N)}$. We design the resolution interval Δ_R between $\mathcal{M}^{(n-1)}$ and $\mathcal{M}^{(n)}$ to be sufficiently small so that the policy $\pi^{(n-1)}$ at the previous resolution can be stably transferred to the next policy $\pi^{(n)}$. The resolution scheduler orders multiple simulation environments, allowing the agent to learn tasks progressively.

B. Policy Learning

1) Execution Flow: An agent collects samples s, a, r from interactions with the simulation and adds them to the rollout buffer $\mathcal{D}^{(n)}$ corresponding to the current resolution. The agent then updates the current policy $\pi^{(n)}$ and current value function $Q^{(n)}$ given $\pi^{(n)}$ using the RL update scheme. At the end of each episode, the success rate τ of the policy is evaluated and passed to the resolution scheduler. When the resolution scheduler updates the resolution Δ , the simulation environments are updated by the simulation generator. Then,

the previous value function $Q^{(n-1)}$ and policy $\pi^{(n-1)}$ are copied to that of the current resolution $Q^{(n)}, \pi^{(n)}$.

PRPD approximately utilizes the conservative policy update scheme to stabilize policy transfer between different resolutions. This scheme was originally developed for a single environment \mathcal{M} in a previous work [18]. This paper approximately utilizes this approach by assuming that a small resolution interval between environments makes these environments similar to a single environment ($\mathcal{M}^{(n)} \approx \mathcal{M}^{(n-1)}$). Therefore, it can be inferred that the lower the similarity (the larger the change in resolution), the lower the effectiveness, which will be verified in detail in Sec. VI-C. For this purpose, we extend the policy linear combination in Eq. (1). Specifically, whereas Eq. (1) conservatively transfers the greedy policy $\mathcal{G}(Q_k)$, PRPD conservatively transfers the learned previous resolution policy $\pi^{(n-1)}$ as following loss function:

$$\begin{cases} \mathcal{L}_{\theta^{(n)}}^{\pi^{(n)}} = \mathbb{E}_{(s,a) \sim \mathcal{D}_i^{(n)}} [\text{KL}\{\pi_k^{(n)}(s, a) || (1 - \alpha_{k+1})\pi_k^{(n)}(s, a) + \alpha_{k+1}\pi^{(n-1)}(s, a)\}], \end{cases} \quad (3)$$

where $\theta^{(n)}$ represents the policy network parameters for the current resolution, and KL denotes the Kullback Leibler divergence.

As shown in Eq. (2), the maximum reward and stationary distribution $d_{\pi, \mu}$ are theoretically necessary for estimating α , but obtaining these parameters in a realistic task is seldom possible. Therefore, we modify Eq. (2) to be able to infer by mini-batch of deep RL by following previous works [18] as:

$$\begin{cases} \alpha_{k+1} = \alpha_0 \mathbb{E}_{s \sim \mathcal{D}_i^{(n)}} [\mathbb{E}_{a' \sim \pi^{(n-1)}(s)} [Q_k^{(n)}(s, a')] - \mathbb{E}_{a \sim \pi_k^{(n)}(s)} [Q_k^{(n)}(s, a)]], \end{cases} \quad (4)$$

where α_0 is a scaling coefficient, $\mathcal{D}^{(n)}$ is the rollout buffer of the current resolution, and k is an update number. Estimated α_{k+1} is utilized by clipping to $[0, 1]$.

Finally, PRPD leverages the dataset $\mathcal{D}^{(n)}$ to train $Q^{(n)}$, parameterized by $\psi^{(n)}$, using the least squares approach typically employed in standard on-policy RL schemes [19]. The current policy $\pi^{(n)}$ is optimized to maximize rewards through the standard on-policy RL framework, utilizing the PPO loss function [19] alongside progressive policy transfer. Overall, the policy network $\theta^{(n)}$ and value network $\psi^{(n)}$ are updated by the summation of the these loss functions.

V. ROCK EXCAVATION

This section outlines the task definition and the simulator developed for learning rock excavation using RL. The objective is to remove various rocks from the ground under different conditions using the bucket. To achieve this, we created both a real-world environment (Fig. 2) and a simulation environment (Fig. 3). We describe the design of excavation motions and sensors optimized with RL and formalize rock excavation as an RL problem.

A. Task Motions

The rock excavation task is defined in three steps: 1) find the rock and move the excavator to it, 2) pick up the

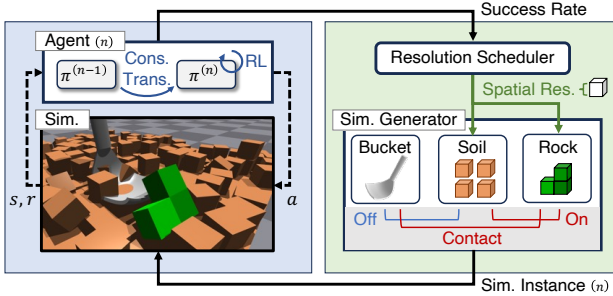


Fig. 3: Applying PRPD to our rock excavation simulator: The resolution scheduler progressively changes the simulation resolution. The simulation generator creates the environment (soil, rocks, bucket) at this resolution. At each resolution, agents collect samples and update policies.

rock from the ground, and 3) dump the scooped rock at a designated place. We focus on learning the pickup operation due to the complexity of soil and rock mechanics. To make the learning process more manageable, we observed human operators and designed parameterized motions for inclining and moving the bucket straight. The incline action allows the bucket to insert into the ground at an angle and tilt to hold the rock, while linear bucket movement helps lift the rock and adjust the relative position between the bucket and the rock. Each motion is optimized with RL.

B. Sensors and Observations

We design three key observations for the excavation task: rock position estimated by the camera, bucket force measured by a force sensor, and bucket position and incline degree recorded by the absolute encoder. Rock position is derived from RGB images and the robot's relative position by estimating the image-based center of gravity. The bucket force observation is represented as a binary value: only the vertical force measured by the sensor is used, with a value of 1 if it exceeds a threshold (indicating contact with a rock or the ground) and 0 otherwise (indicating the bucket is in the air). The bucket's incline is limited to the scooping direction to reduce action dimensions and, if the torque limit is exceeded, the arm's movement in that direction is restricted. Each observation is recorded once at the end of the agent's action and is used as the next agent's observation.

C. Learning Formulation

We formulate this rock excavation as an RL problem. The observation s is defined from the estimated rock posture (XY position and pitch rotation) p^r , the estimated rock force f^r , and bucket position p^b , $s = [p^r, f^r, p^b]$. As supplementary information, soil details (such as appearance and particle count) differ between resolutions and exceed the assumptions of the proposed framework; to enable policy transfer across different resolutions, these details are excluded from observations. The action a is defined as $a = [a^{XYZ}, a^{Pitch}]$: a^{XYZ} is the move straight bucket action that represents the relative XYZ position of the bucket and a^{Pitch} is the inclining bucket action that represents the relative pitch angle of the bucket. Both a^{XYZ} and a^{Pitch} are executed simultaneously at every step t . The reward r is defined from the current rock height h^{rock} , $r = h^{rock}$. The task success is evaluated by determining

TABLE I: Calculation time per one-step sample in each resolution.

Res. Δ [mm]	70	60	50	40	30	20	10
Time [ms]	0.24	0.26	0.34	0.41	0.94	2.97	5.03

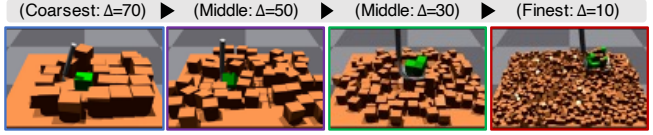


Fig. 4: Snapshots of simulation environments with each resolution

whether the rocks are above ground height h^{ground} using the following indicator function: $\mathbb{I}(h^{rock} > h^{ground})$.

D. Variable Resolution Simulator

We designed and implemented a variable-resolution simulator for rock excavation tasks using Isaac Gym. The simulator is presented in Fig. 3 and enables us to remove the various rocks on various ground types by inclining and moving the bucket. The excavator's whole body model and the process of moving the excavator to the rocks and putting the rocks in other places are excluded. The rock position is obtained directly by the simulation property. 3D CAD software was utilized to design the bucket. The shape of the ground soil particle was assumed to be a box. The bucket was designed to make contact only with the rock, eliminating resistance to particles representing soil; this is for the purpose of expressing that the fork-shaped bucket can move and dig out the soil.

Our rock-excavation simulator generates environments containing soil and rocks based on the specified simulation resolution Δ . In this paper, we focus on spatial resolution, dynamically adjusting parameters such as soil particle size and count, and rock shape precision. Rock resolution has minimal impact on simulation time but is included in the resolution to progressively increase task difficulty, as higher resolutions represent more complex shapes. For soil, particles are generated as boxes with side lengths represented by resolution Δ to match a predefined total soil volume. Rocks are represented as a collection of connected boxes. Specifically, boxes with side lengths represented by resolution Δ are connected face-to-face until the defined rock volume is reached. To create diverse rock shapes, the faces of the connected boxes are randomly selected.

The calculation times and environment snapshots at different resolutions for our developed simulator are shown in Table I and Fig. 4, respectively. The calculation time of this simulator improves as resolution Δ becomes finer due to more soil particles and complex rock shapes, which result in more contact points and higher calculation times, as well as increased GPU memory usage. Consequently, finer-resolution simulations require significant calculation time, making the collection of the vast number of learning samples needed for RL very challenging.

VI. EXPERIMENTS

We conducted experiments to validate the following objectives. PRPD can learn policies in a shorter learning time compared to previous works (Sec. VI-B). The conservative policy

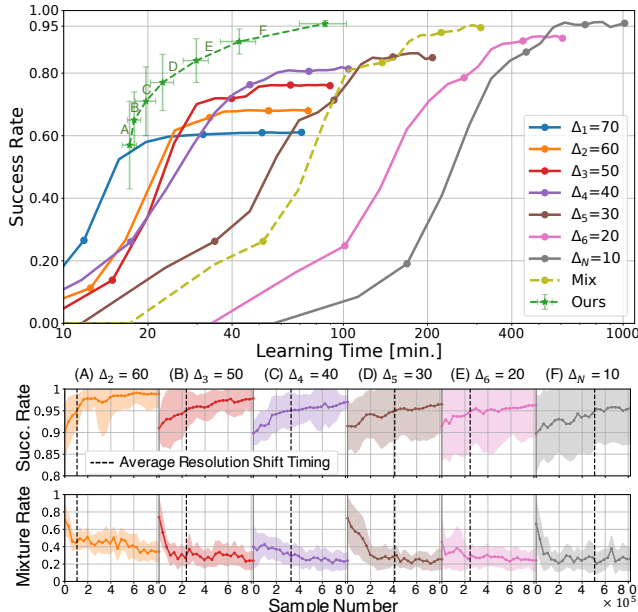


Fig. 5: Comparison of learning time (top) and policy mixture rate (bottom). **(Top)** This compares learning time between fixed resolution learning and PRPD. $\Delta = 70, \dots, \Delta = 10$ refers to resolutions as Table I, while “Mix” refers to mixed resolutions (simultaneous policy learning), both up to $400 \times 128 \times 128$ samples (circle points are plotted every $100 \times 128 \times 128$ samples). The success rate is evaluated 100 times in $\Delta = 10$ at each iteration. **(Bottom)** This shows the task success rate and mixture rate transitions of PRPD in each resolution. The dashed line indicates when the scheduler changes resolution by achieving the target success rate $\hat{\tau}$. $\Delta = 70$ is the initial environment and lacks a previous policy, so the mixture rate is omitted. Each curve plots the mean (and variance) over five experiments.

transfer scheme stabilizes learning in PRPD (Sec. VI-C). Differences in resolution scheduling affect policy learning (Sec. VI-D). Trade-off between time efficiency and sample efficiency compared to other RL methods (Sec. VI-E). The policy trained in the simulator can be applied to various real-world environments (Sec. VI-F).

A. Common Settings

The experiments used a Universal Robots UR5e manipulator to control rocks with a bucket. Rock position was estimated using an Intel RealSense Depth Camera D435 and bucket force was measured with a Robotiq FT 300-S Force Torque Sensor. The robot controlled the fingertip pose at approximately 100 Hz. In all experiments, the learning parameter settings follow those of previous works, including learning parameters [19] and network architectures [20]. Detailed parameter settings are available on the project pages: <https://yuki-kadokawa.github.io/prpd/>. Policy learning utilized PPO with parallel environments, where the number of parallel environments was determined by the maximum that could be calculated on the PC setup (Intel Core i9-9900X CPU and GeForce RTX 3090 GPU) for the highest resolution environment ($\Delta = 10$). For real-world evaluation, nine rocks of varying shapes and sizes were used, as shown in Table II.

This paper applies a domain randomization (DR) technique [20] to learn robust policies for reality gaps between the simulation and the real world. The learned policy is then utilized in real-world environments without additional learning costs. We randomized simulation parameters during

training as described in the project pages. These parameters were uniformly randomized at every episode.

This experiment evaluates three key aspects. **Sample number** is defined as the total number of samples collected by the policy. **Success rate** is defined as the percentage of episodes per iteration that achieve the task, with success defined in Sec. V-C. **Learning time** is defined as the total training time, including both environment interactions and policy optimization.

B. Effect of Resolution Scheduling for Short-time Learning

1) *Settings*: PRPD schedules simulation resolution for short-time policy learning in fine-resolution simulations. To verify its effectiveness, we compare the learning time and performance between PRPD and the policy learning conducted in a fine-resolution simulation. Additionally, policy learning in only coarse-resolution simulations may achieve high performance in a shorter time. Thus, we evaluate policy learning with fixed coarse-resolutions in various patterns of resolutions. In addition, policy learning in various resolutions simultaneously may be more efficient than scheduling resolutions. This framework is also compared.

2) *Results*: As shown in Fig. 5, PRPD learns control policies in less than one-seventh of the time needed to reach the highest success rate compared to fixed resolution learning. Coarser resolutions result in faster convergence, with a 20-fold difference in learning time between $\Delta = 70$ and $\Delta = 10$, but they also reduce performance by about 35%. PRPD converges in less than one-fourth of the time compared to simultaneous learning across all resolutions. These results demonstrate that the proposed resolution scheduling framework achieves the fastest policy learning.

C. Effect of Conservative Policy Transfer

1) *Settings*: PRPD applies a conservative policy transfer scheme to stabilize policy transfers caused by progressive resolution shifts. Specifically, the learning is stabilized by dynamically optimizing the mixture rate α (Eq. (4)). To evaluate the effectiveness of optimizing α , we compared its performance with other baselines with constant α .

2) *Results*: As shown in Fig. 6(a), $\alpha = \text{opt.}$ achieves the shortest learning time compared to fixed mixture rates. Additionally, $\alpha = 1$, where previous policies $\pi^{(n-1)}$ are used without optimization, outperforms $\alpha = 0$, which does not use previous policies. These results confirm that the conservative policy transfer scheme enables learning with fewer samples.

From the transition of the policy mixture rate α in PRPD shown in Fig. 5, α tends to be high in the early learning iterations of each resolution. This denotes that, during the initial phase of progressive resolution shifts, the update of the current policy $\pi^{(n)}$ is unstable and stronger regularization is added to prevent extensive updates from the previous policy $\pi^{(n-1)}$. As learning progresses, the update of $\pi^{(n)}$ stabilizes and the regularization decreases.

D. Influence of Different Resolution Scheduling

1) *Settings*: Since PRPD defines the resolution scheduler deciding learning resolution in a certain resolution interval

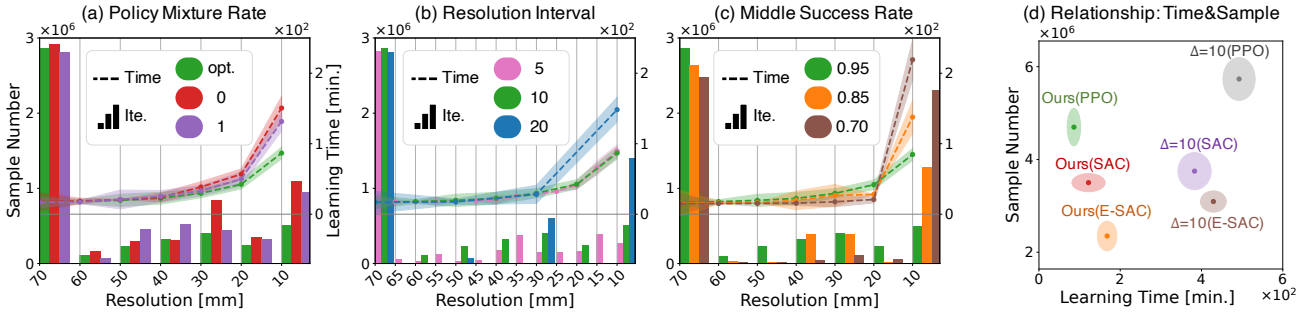


Fig. 6: Summaries of analysis: **(Left)** Performance comparison of PRPD components for (a) different patterns of policy mixture rate, (b) different numbers of target middle success rate, and (c) different numbers of target middle success rate. The box plots represent the sample numbers at which the policies achieve the target success rate $\hat{\tau}$ for each resolution. The dashed lines denote the total learning time from the initial resolution to the plotted resolution. α denotes the policy mixture rate, which is dynamically updated only in $\alpha = \text{opt.}$ **(Right)** (d) Relationship between learning time and number of samples in policy learning required to reach $\hat{\tau}$. Each curve and point of (a), (b), (c), and (d) plots the mean and variance per sample over five experiments (each box plot plots the mean). The learning sample is the value until the target success rate $\hat{\tau}$ is reached at the corresponding resolution (for Ours in (d), it is the summation value until $\hat{\tau}$ is reached at the final resolution $\Delta = 10$).

Δ_R , the interval must be small enough to ensure a successful policy transfer. Also, as the resolution scheduler decides target success rates $\hat{\tau}$ for shifting resolution, the target middle success rates, the ones used except for the final resolution, may influence sample efficiency since middle tasks are not needed to solve perfectly. Thus, we investigate the performance of PRPD with various Δ_R and τ .

2) *Results:* As shown in Fig. 6(b), when the interval is coarse, the sample efficiency is poor, requiring about 1.5 times more samples. However, making the interval finer does not always improve efficiency, as there is almost no difference in sample efficiency when $\Delta_R = 10$ or less. This indicates that there is an optimal interval range where policy transfer works effectively. As shown in Fig. 6(c), lowering the target middle success rate τ requires more samples. This suggests that policy transfer is ineffective before the policy acquires sufficient skills.

E. Tradeoff between Time-Efficiency and Sample-Efficiency

1) *Settings:* As mentioned in Sec. II-C, various methods have enhanced RL’s sample efficiency, but less attention has been given to “time efficiency.” This section demonstrates that the proposed method outperforms previous sample-efficient approaches in terms of time efficiency. SAC [16] and its ensemble variant E-SAC [14] were evaluated within the PRPD and finest fixed-resolution with $\Delta = 10$.

2) *Results:* As shown in Fig. 6(d), the proposed PRPD framework outperforms the fixed resolution $\Delta = 10$ in terms of time efficiency across all RL methods. Ours (PPO) reached target success rate $\hat{\tau}$ at the finest resolution $\Delta = 10$ in less than 100 minutes, significantly faster than the training in only finest resolution $\Delta = 10$ (PPO), which took about 500 minutes. The extremely slow simulation at $\Delta = 10$ made the $\Delta = 10$ (PPO) less time-efficient than sample-efficient methods, as the sampling cost outweighed the policy optimization cost. Comparing ours (SAC) with $\Delta = 10$ (SAC), there is little difference in sample numbers, but the learning time shows over a twofold difference, demonstrating that the progressive resolution shift significantly enhanced time efficiency.

F. Sim-to-Real Policy Transfer

This section validates the sim-to-real policy transfer across diverse real-world rock-excavation environments, including silica sand (low viscosity), kinetic sand (high viscosity), and plastic pellets (blocky shape and large grain size). Table II displays the evaluation of the transfer policies. The experiment shows that the success rate increases as the resolution improves in the real-world environment for fixed resolution policies, as was demonstrated with the simulation results. PRPD achieves performance comparable to fine-resolution fixed policy learning, indicating no adverse effects from using coarse-resolution simulations and successful sim-to-real transfer. We also evaluated the differences in policy performance during sim-to-real transfer depending on the presence of DR parameters. Table II shows that policy performance dropped to approximately 50 % without DR. This indicates a reality gap between the simulation and real-world environments, mitigated by applying DR. These results demonstrate that the variable-resolution rock excavation simulator and the proposed policy learning framework achieve approximately 90 % success rates for nine types of real rock environments.

VII. DISCUSSIONS

Finer resolution assumption: In this paper, we assumed that finer resolution in excavation simulators leads to better transfer policy performance in real-world environments, supported by the experimental results in Sec. VI-F. However, this assumption may not always hold. The relationship between resolution and the reality gap is complex, as finer resolution may sometimes widen the gap. Moreover, when combined with domain randomization, simulators with relatively coarser resolution may enhance the learned policy’s performance and generalization.

Automatic determination of resolution interval: As an extension of the proposed PRPD, automatic determination of resolution intervals Δ_R could be considered. In Sec. VI-D, we showed that finer Δ_R allows for learning with fewer samples. Since these parameters depend on the task and policy learning algorithm, determining a single optimal value is difficult. However, developing a framework to automatically

TABLE II: Sim-to-real experiment of rock excavation: This experiment evaluated nine types of rocks (five differently shaped wooden blocks and three different-sized 3D-printed artificial rocks as shown in rock images) on three types of ground (for each element, three numbers correspond to each environment, silica sand, kinetic sand, and plastic pellets in order). “Scale” indicates approximate rock size. The first-row block shows “Ours” (PRPD) and “w/o DR” (PRPD without DR). The second-row block shows PPO at a fixed resolution. Each value indicates the success number per 20 trials, with the last column showing the average rate. The 20 trials test five policies at four positions (0, 60, 120, and 180 degrees) on a 100-mm radius circumference relative to the bucket’s initial position. Task success is defined as rocks being held in the bucket and the bucket being off the ground.

Rock Image										Ave.
Scale [mm ³]	50x50x50	75x75x75	100x100x50	100x50x50	100x100x50	100x100x50	140x70x70	160x80x80	180x90x90	[%]
Ours	19-19-20	17-14-16	18-18-15	20-19-20	19-17-19	18-17-14	19-20-18	18-16-16	18-15-17	88.1
w/o DR	16-14-18	11-11-9	15-13-14	16-16-17	14-13-12	5-4-7	12-10-6	9-6-3	3-4-1	51.7
$\Delta = 10$	20-19-19	19-15-17	18-17-18	20-19-19	18-16-17	17-15-16	18-19-18	19-18-16	18-16-17	88.5
$\Delta = 20$	19-16-20	20-13-20	17-14-16	19-17-18	18-14-20	16-15-12	19-16-18	18-14-17	15-14-14	83.1
$\Delta = 30$	19-17-18	19-12-19	16-16-15	19-20-19	17-15-16	15-15-12	17-16-14	18-15-16	13-12-10	79.6
$\Delta = 40$	19-19-19	16-10-17	17-18-16	18-19-16	18-15-16	13-14-13	18-15-15	20-12-18	11-11-9	78.1
$\Delta = 50$	20-18-20	17-11-15	14-11-12	18-19-19	14-11-15	14-15-9	17-14-14	16-13-13	12-11-11	72.8
$\Delta = 60$	17-15-17	15-12-15	13-11-10	20-18-18	16-13-17	10-9-7	19-17-17	15-9-11	6-5-6	66.3
$\Delta = 70$	18-18-20	15-10-16	14-9-13	17-16-19	16-12-15	9-10-4	18-16-16	14-9-13	3-3-4	64.3

adjust simulation intervals based on their relationship would be beneficial.

Applicability of proposed framework: This paper focuses on rock excavation within earthwork tasks, developing a simulator and a learning algorithm. PRPD, which progressively changes simulation resolution, could extend to other excavation tasks or the installation of non-rock objects. It may also apply to tasks where simulation resolution impacts simulation time beyond earthwork. As shown in Fig. 5, this study achieved a 7-fold improvement in learning time efficiency, an approximately 8-hour time gap. This time gap may grow with increasing task complexity or state-action space. Using finer resolutions than $\Delta = 10$ could further widen the learning time difference.

VIII. CONCLUSION

In this paper, we proposed time-efficient policy learning framework PRPD to address the time inefficiency of a fine-resolution rock-excavation simulator. We evaluated PRPD by developing a variable-resolution rock-excavation simulator using Isaac Gym. PRPD significantly reduced policy learning time in the simulator. Additionally, the learned policy was successfully transferred to the real-world environment, robustly removing previously unseen rocks.

REFERENCES

- [1] D. Lee, I. Jang, J. Byun, H. Seo, and H. J. Kim, “Real-Time Motion Planning of a Hydraulic Excavator Using Trajectory Optimization and Model Predictive Control,” in *IEEE/RSJ International Conference on Intelligent Robots and Systems*, 2021, pp. 2135–2142.
- [2] L. Zhang, J. Zhao, P. Long, L. Wang, L. Qian, F. Lu, X. Song, and D. Manocha, “An Autonomous Excavator System for Material Loading Tasks,” *Science Robotics*, vol. 6, no. 55, 2021, eabc3164.
- [3] S. Dadhich, U. Bodin, and U. Andersson, “Key Challenges in Automation of Earth-Moving Machines,” *Automation in Construction*, vol. 68, pp. 212–222, 2016.
- [4] C. Tampier, M. Mascaro, and J. Ruiz-del Solar, “Autonomous Loading System for Load-Haul-Dump (LHD) Machines Used in Underground Mining,” *Applied Sciences*, vol. 11, no. 18, 2021, 8718.
- [5] F. E. Sotiroopoulos and H. H. Asada, “Autonomous Excavation of Rocks Using a Gaussian Process Model and Unscented Kalman Filter,” *IEEE Robotics and Automation Letters*, vol. 5, no. 2, pp. 2491–2497, 2020.
- [6] S. E. Li, “Deep Reinforcement Learning,” in *Reinforcement Learning for Sequential Decision and Optimal Control*, 2023, pp. 365–402.
- [7] D. Jud, P. Leemann, S. Kerscher, and M. Hutter, “Autonomous Free-Form Trenching Using a Walking Excavator,” *IEEE Robotics and Automation Letters*, vol. 4, no. 4, pp. 3208–3215, 2019.
- [8] K. Matsumoto, A. Yamaguchi, T. Oka, M. Yasumoto, S. Hara, M. Iida, and M. Teichmann, “Simulation-Based Reinforcement Learning Approach Towards Construction Machine Automation,” in *Proceedings of the International Symposium on Automation and Robotics in Construction*, vol. 37, 2020, pp. 457–464.
- [9] H. Tahara, H. Sasaki, H. Oh, B. Michael, and T. Matsubara, “Disturbance-Injected Robust Imitation Learning with Task Achievement,” in *International Conference on Robotics and Automation*, 2022, pp. 2466–2472.
- [10] A. Haeri and K. Skonieczny, “Three-Dimensional Granular Flow Continuum Modeling via Material Point Method with Hyperelastic Nonlocal Granular Fluidity,” *Computer Methods in Applied Mechanics and Engineering*, vol. 394, p. 114904, 2022.
- [11] Y. Kadokawa, M. Hamaya, and K. Tanaka, “Learning Robotic Powder Weighing from Simulation for Laboratory Automation,” in *IEEE/RSJ International Conference on Intelligent Robots and Systems*, 2023, pp. 2932–2939.
- [12] D. Millard, D. Pastor, J. Bowkett, P. Backes, and G. S. Sukhatme, “GranularGym: High Performance Simulation for Robotic Tasks with Granular Materials,” in *Robotics: Science and Systems*, 2023.
- [13] M. Okada and T. Taniguchi, “Dreaming: Model-Based Reinforcement Learning by Latent Imagination Without Reconstruction,” in *International Conference on Robotics and Automation*, 2021, pp. 4209–4215.
- [14] M. R. Maulana and W. S. Lee, “Ensemble and Auxiliary Tasks for Data-Efficient Deep Reinforcement Learning,” in *Joint European Conference on Machine Learning and Knowledge Discovery in Databases*, 2021, pp. 122–138.
- [15] D. Yarats, I. Kostrikov, and R. Fergus, “Image Augmentation is All You Need: Regularizing Deep Reinforcement Learning from Pixels,” in *International Conference on Learning Representations*, 2021.
- [16] T. Haarnoja, A. Zhou, P. Abbeel, and S. Levine, “Soft Actor-Critic: Off-Policy Maximum Entropy Deep Reinforcement Learning with a Stochastic Actor,” in *International Conference on Machine Learning*, 2018, pp. 1861–1870.
- [17] S. Narvekar, B. Peng, M. Leonetti, J. Sinapov, M. E. Taylor, and P. Stone, “Curriculum Learning for Reinforcement Learning Domains: A Framework and Survey,” *Journal of Machine Learning Research*, vol. 21, no. 181, pp. 1–50, 2020.
- [18] N. Vieillard, O. Pietquin, and M. Geist, “Deep Conservative Policy Iteration,” in *Association for the Advancement of Artificial Intelligence*, 2020, pp. 6070–6077.
- [19] J. Schulman, F. Wolski, P. Dhariwal, A. Radford, and O. Klimov, “Proximal Policy Optimization Algorithms,” *arXiv preprint arXiv:1707.06347*, 2017.
- [20] X. B. Peng, M. Andrychowicz, W. Zaremba, and P. Abbeel, “Sim-to-Real Transfer of Robotic Control with Dynamics Randomization,” in *IEEE International Conference on Robotics and Automation*, 2018, pp. 3803–3810.